

Numerical modelling of FRP strengthened RC beam-column joints

Seyed S. Mahini[†]

Department of Civil Engineering, Yazd University, Yazd, Iran

Hamid R. Ronagh[‡]

Division of Civil Engineering, School of Engineering, The University of Queensland, Brisbane, QLD 4072, Australia

(Received February 15, 2007, Accepted June 15, 2009)

Abstract. This paper reports part of a comprehensive research study conducted at the University of Queensland on the ability of CFRP web-bonded systems in strengthening an exterior beam-column joint subjected to monotonic loads. One 1/2.2 scaled plain and four CFRP repaired/retrofitted joints subjected to monotonic loads were analysed using the nonlinear finite-element program ANSYS and the results were calibrated against experiments. The ANSYS model was employed in order to account for tension stiffening in concrete after cracking and a modified version of the Hognestad's model was used to model the concrete compressive strength. The stress-strain properties of main steel bars were modelled using multilinear isotropic hardening model and the FRPs were modelled as anisotropic materials. A perfect bond was assumed as nodes were shared between adjacent elements irrespective of their type. Good agreement between the numerical predictions and the experimental observation of the failure mechanisms for all specimens were observed. Closeness of these results proved that the numerical analysis can be used by design engineers for the analysis of web-bonded FRP strengthened beam-column joints with confidence.

Keywords: reinforced concrete; joints; strengthening; fibre reinforced plastics; finite element method; nonlinear analysis.

1. Introduction

Studying the damage patterns of reinforced concrete structures damaged in recent earthquakes have indicated that beam-column joints may be critical regions that require upgrade and strengthening. It has been reported that in no other comparable event have as many beam-column joint failures been observed as in the 1980 El Asnam earthquake. Shear and anchorage failures, particularly at exterior joints, have also been identified after 1985 Mexico, 1986 San Salvador, and 1989 Loma Prieta earthquakes (Paulay and Priestley 1992).

[†] Assistant Professor, E-mail: s.mahini@yazduni.ac.ir

[‡] Senior Lecturer, Corresponding author, E-mail: h.ronagh@uq.edu.au

It is universally accepted that a good strategy for designing earthquake resistant frames is the implementation of the *weak-beam strong-column* concept. This way, the joint is designed in such a way that the joint core and the column remain elastic under lateral loads while adequate energy dissipation occurs through plastic deformation at the beam's end. The damage would then be concentrated at the beam's end of the joint. This will ensure that any future repair would also be concentrated at the beam's end and as such is easy to repair and cost-effective. Rehabilitation may become necessary when joints lack sufficient strength, stiffness or ductility. In recent years, a significant amount of research studies have been devoted to strengthening techniques incorporating advanced composite materials such as FRPs. The majority of studies on strengthening of RC joints have been concentrated on the shear strengthening of the joint core. Only a few studies were performed on upgrading the flexural capacity the beam-column joint.

Numerical investigations on the joint and joint rehabilitation are extremely limited. Kwak and Fillippou (1990) made use of finite element analysis in order to study monotonically loaded reinforced concrete beam-column joints. Their model was capable of considering crushing and cracking of concrete. Kwak and Fillippou (1990) proposed a new smeared finite element model based on an improved cracking criterion, which was derived from fracture mechanics principles. They also developed a new reinforcing steel model, which was embedded inside a concrete element and could account for the effect of bond-slip. Kwak and Fillippou (1990) performed correlation studies between analytical and experimental results. Several parametrical studies were also conducted with the objective of checking the validity of proposed models and identifying the significance of various parameters on the local and global response of reinforced concrete joints. A numerical study of the behaviour of exterior beam-column joints using ANSYS was performed by Vollum (1998). The influence of varying the element size, shear transfer coefficient for open cracks, modelling of reinforcement and load step and convergence criteria were investigated in this study. Vollum (1998) modelled concrete by ANSYS solid element (Solid65), which is an 8-node brick element that employs William and Warnke (1975) model for the triaxial behaviour of concrete. The steel reinforcements were modelled by link elements that were connected to the nodes of the solid elements. In another effort, Baglin and Scott (2000) used a nonlinear finite element software (SBETA) for the modelling of exterior beam-column joints. The software provided the user with first-order quadrilateral elements only. The concrete was modelled by defining the compression strain-softening curve and the steel through a bilinear strain-stress relation. They compared the behaviour of the finite element model with the results of 19 experimental tests. A parametric study was conducted in order to evaluate the effects of main variables on both the joint capacity and the joint behaviour and the effects of column load on joint details.

A parametric investigation into the application of FRP composite laminates to exterior beam-column joints was carried out by Parvin and Granata (2000) in order to investigate the increase of flexural capacity under monotonic loads. Nonlinear finite element analysis of three beam-column joints with laminates bonded to the tensile faces of the beam-end were carried out in their investigation. Parvin and Granata (2000) again modelled the concrete using ANSYS (solid65). They used a two-noded link element (link8) for modelling the reinforcing steel and also an eight-node three-dimensional multi layer solid element (solid45) for FRPs. Parvin and Granata indicated that the fibre composite types, the laminate and wraps' arrangement and thickness affect the joint capacity significantly. They observed an increase in the moment capacity of up to 37% in their investigation.

The ANSYS finite element program (ANSYS 2003) is used in this study to simulate the

behaviour of beam-column specimens tested by Mahini *et al.* (2004) and Ronagh and Mahini (2005). An overview of the experiments is given next followed by the numerical modelling and the results.

2. Experiments

The emphasis of this paper is the nonlinear FE analyses and therefore experiments are only briefly described. More details can be found in Mahini *et al.* (2004), Ronagh and Mahini (2005) and Mahini and Ronagh (2006). The test specimens were five 1:2.2 scale models of the prototype. The prototype structure was a typical eight story residential RC building located in Brisbane. The controlling design criterion for this structure was the strength required to resist the applied gravity and lateral loads. The prototype was designed as an Ordinary Moment Resisting Frame (OMRF), according to the Australian Concrete Code AS 3600 (2001), with details similar to non-ductile RC frames designed to ACI-318 (2002), American standard. A scaled-down frame was modelled by the application of the similitude requirements that relate the model to the prototype using the Buckingham theorem (Noor and Boswell 1992). The scaled-down joints were extended to the column mid-height and beam mid-span, corresponding to the inflection points of the bending moment diagram under lateral loading. Code provisions were used to determine the spacing of steel stirrups and ties. The specimen size and reinforcement were limited by the hydraulic actuator size and the ultimate capacity of hydraulic jacks that apply the loads to the column and the testing frame. The specimens were tested in a 2D testing frame. This test frame was equipped with a hydraulic actuator of 100 kN capacity and a hydraulic jack with a maximum capacity of 500 kN. The loading was applied monotonically by the actuator, which was capable of applying loads in both load and displacement control regimes. Load and deflections were automatically recorded using a computerized data acquisition system. Lateral loads were applied to the beam tip using the hydraulic actuator. A constant 305 kN load was applied to the column using the hydraulic jack. The load control regime was used to capture the steel reinforcement yielding point. After yielding, the test was continued using a displacement control regime up to displacements that were corresponding to a ductility factor of 5.

Fig. 1 shows the specimens' details. Cross-sectional dimensions of beams and columns were 180 by 230 mm and 180 by 220 mm respectively. Four N12 rebars ($\phi 12$ mm) were used for both the column vertical reinforcement and the beam longitudinal reinforcement. R6.5 bars ($\phi 6.5$ mm) were used for stirrups with a spacing of 150 mm in both column and beam. The joint detail was designed according to AS3600. The control specimen, CSM0 was tested to failure under a monotonic load regime. Two other specimens, RPSM1 and RPSM2 were pre-cracked, repaired and then retested under a similar loading regime. Two undamaged specimens, RSM1 and RSM2, were retrofitted and tested under the same loading regime as repaired specimens, RPSM1 and RSM2 to failure.

Carbon Fibre Reinforced Polymer (CFRP) sheets that were used in the experiments were uni-directional. The sheets were glued to the web of the beam with the fibre orientation parallel to the beams' longitudinal axis. The beams were not fully wrapped as it could have been impractical in real situations due to the interface with the concrete slab. Wraps were extended over the joint core area to the back of the column in order to minimize the possibility of premature delamination.

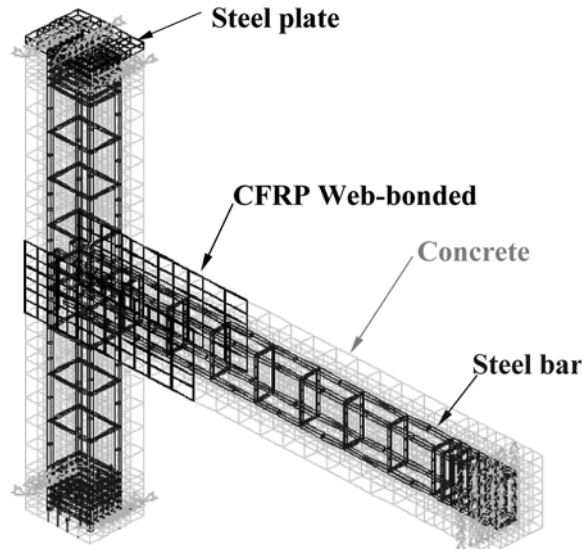


Fig. 2 Typical FE mesh of the CFRP- repaired/retrofitted specimen

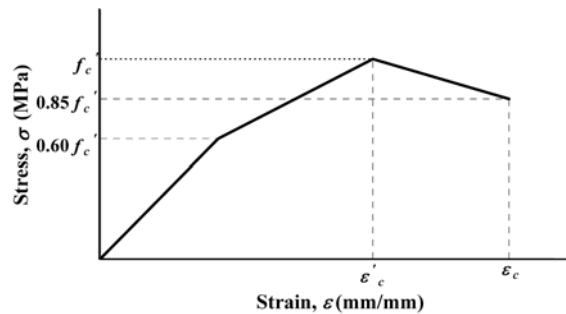


Fig. 3 Concrete stress-strain relation used for all specimens (Kwak and Fillippou 1990)

Ideally, a partial bond between concrete and steel reinforcements should be considered. However, perfect bond between materials is usually assumed. To provide the perfect bond, the link element used for steel reinforcements was connected between the nodes of adjacent concrete solid elements, so that the two materials shared the same nodes. The same approach was employed for FRP composites assuming that a high strength epoxy is used to attach FRP sheets to the RC joints areas. Nodes of the FRP solid elements were connected to those of adjacent concrete solid elements in order to satisfy the perfect bond assumption.

The concrete is modelled by solid65. Solid65 allows the presence of four different materials within the concrete element; one matrix material, and a maximum of three independent reinforcing materials that are assumed to be smeared throughout the element.

A modified version of the Hognestad’s model developed by Kawak and Fillippou (1990) is used, as shown in Fig. 3. As is seen, ϵ'_c is the strain corresponding to the concrete compressive strength f'_c under uniaxial stress conditions and is taken as 0.002 as recommended by Park and Paulay (1975) for normal concrete. Also, the value of ϵ_{cu} is taken as 0.003 for all concrete pours, as recommended by AS3600.

Both cracking and crushing failure modes are accounted for the concrete model in ANSYS. To define a failure surface for concrete, two strength parameters, i.e., ultimate tensile and compressive strengths, are needed. During this study, it was found that when the crushing capability of the concrete is turned on, the finite element beam models fail prematurely. As, a pure compression failure of concrete is unlikely, the crushing capability is turned off and therefore cracking of concrete controlled the failure of the finite element models.

FEM input data for the solid65 element are Elastic modulus, E_c , ultimate uniaxial compressive strength, f'_c , ultimate uniaxial tensile strength, f_r , Poisson's ratio, ν_c , for concrete, shear transfer coefficients, β_i and β_c and compressive uniaxial stress-strain relationship for concrete.

The elastic modulus of concrete; E_c , can be estimated from standard tests. In AS3600, the ultimate uniaxial compressive and tensile strength of concrete can be traced back to the elastic modulus and compressive strength using Eqs. (1) and (2) respectively

$$f'_c = \left(\frac{E_c}{0.043\rho^{1.5}} \right)^2 \quad (1)$$

$$f_r = 0.6\sqrt{f'_c} \quad (2)$$

where E_c , f'_c , and f_r are in MPa and ρ is the density of the concrete in kg/m³. Poisson's ratio, ν_c , for concrete was assumed 0.2 for the beam elements.

In this study, the ultimate uniaxial compressive strength, f'_c , and the elastic modulus of concrete, E_c , were obtained from standard compression tests on concrete cylinders. The ultimate uniaxial tensile strength, f_r , was calculated using Eq. (2) for FE analysis of all specimens and Poisson's ratio was taken as 0.2. The concrete has a compressive strength around 40, 52, 48, 45 and 40.75 MPa and a modulus of elasticity around 27.6, 35.7, 35.2, 29.4 and 30.9 GPa for plain (CSM0), repaired specimens (RPSM1 and RPSM2) and retrofitted specimens (RSM1 and RSM2) respectively.

The presence of a crack at an integration point is taken into account through modification of the stress-strain relations by introducing a plane of weakness in a direction normal to the crack face. Also, a shear transfer coefficient, β_s , is introduced which represents a shear strength reduction factor (i.e., shear transfer coefficient) for those subsequent loads, which induce sliding (shear) across the crack face. If the crack closes, then all compressive stresses normal to the crack plane are transmitted across the crack and only a shear transfer coefficient, β_c , for a closed crack is introduced. In other words, the shear transfer coefficients, β_i and β_c , represent conditions of the crack and depending on opening or closing, vary the shear strength across the crack. These values range from zero for a smooth crack (complete loss of shear transfer) to one for a rough crack (no loss of shear transfer). Previous researchers have chosen values of β_i between 0.05 and 0.5. In the current study, the best estimates of the behaviour are obtained if a shear transfer coefficient, β_s , of 0.3 is taken for open cracks. The shear transfer coefficient for closed cracks, β_c , is taken as 0.7, as recommended in the ANSYS online manual. Fig. 4 shows the ANSYS model accounting of tension stiffening in concrete after cracking. The required input is the slope (secant modulus), R^1 as defined in this figure. R^1 works with adaptive drop and reduces to 0.0 when the solution converges.

Other parameters used in the modelling are f_t which is the uniaxial tensile cracking stress and T_c that is the multiplier for the amount of tensile stress relaxation. This has a default value of 0.6.

In addition to the rebar capability of the solid65 element, the reinforcing steel can be modelled in ANSYS using a series of two node link (truss) elements, called link8, which has three translational

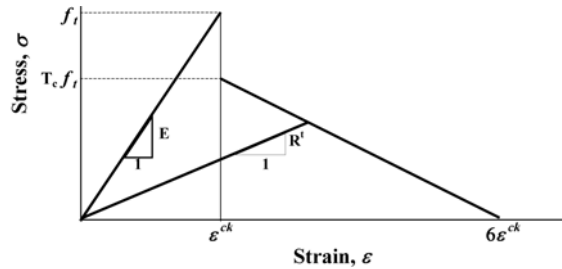


Fig. 4 Strength of cracked condition

degrees of freedom and is capable of plastic deformations. In the current study, all steel bars and stirrups are modelled using the link8 element.

As mentioned previously, two types of the reinforcements, N12 and R6.5, were used in this study. In order to model the behaviour of the deformed steel reinforcement, several standard tests were carried out on the actual samples of the reinforcements that were used for fabrication of the specimens and an average of the test results was used to model the stress-strain curve of the steel reinforcements using multilinear modelling. For this, the nonlinear stress-strain relation was approximated by a series of straight line segments meeting at the critical points, such as the onset of steel yielding and strain hardening. Yield strength of the main steel reinforcements, N12 and the stirrups R6.5 were around 500 MPa and 382 MPa respectively with a modulus of elasticity about 200 GPa. The Poisson’s ratio, ν_s of both reinforcements was about 0.3.

FEM input data for all steel bars are Elastic modulus, E_s and Poisson’s ratio, ν_s . For modelling the stress-strain properties of N12 steel bars, the ANSYS Multilinear Isotropic Hardening command was used as shown in Fig. 5. For this, stresses and strains of the steel at each straight line segments were required. For R6.5 stirrups, a bilinear model with a zero strain hardening modulus was used (see Fig. 5).

In ANSYS, FRP composites can be modelled using an eight-node 3D solid element called SOLID45. This element is defined by eight nodes each having three translational degrees of freedom. In addition to FRPs, in this study, Solid45 is used for the steel plates, which are added at the support locations of the column simulating the actual set-up.

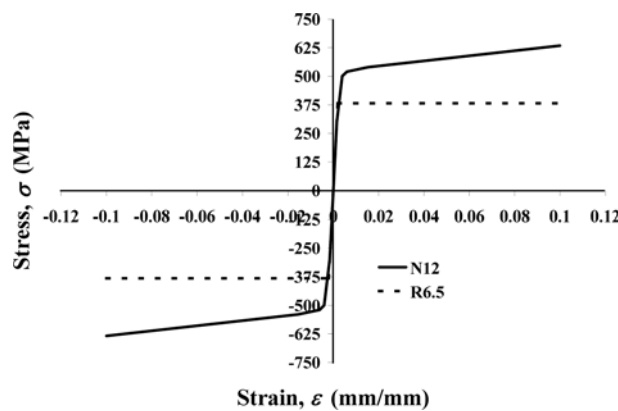


Fig. 5 Stress-strain curve for deformed bars, N12 and stirrups, R6.5

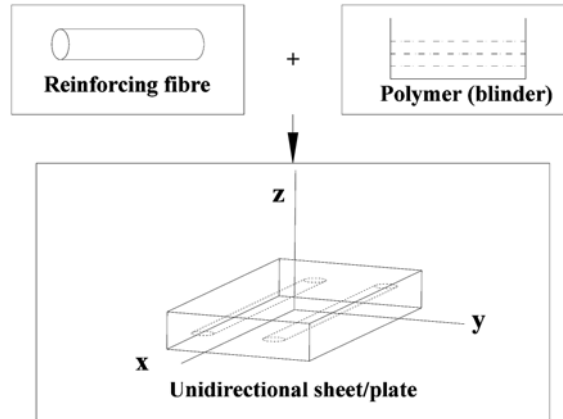


Fig. 6 Schematic of FRP composites (Kachlakev *et al.* 2001)

FRP composites are materials that contain two ingredients. The constituents are combined macroscopically and are not soluble in each other. These are the reinforcement and a continuous polymer called the matrix. The reinforcing material is in the shape of fibres (i.e., carbon and glass), which are typically stiffer and stronger than the matrix. The FRP composites are anisotropic materials; that is, their properties are different in all directions. A schematic of FRP composites is shown in Fig. 6. As is seen, a unidirectional sheet has three orthogonal planes of material properties (i.e., x - y , x - z , and y - z planes). The xyz coordinate axes are referred to as the principal material coordinates, where the x direction is the same as the fibre direction, and the y and z directions are perpendicular to the x direction. It is a so-called especially orthotropic material (Kachlakev *et al.* 2001).

Typically, the volume fraction of fibres in FRPs is about 50-70 percent for strips and about 25-35 percent for sheets. Hence, fibres are the principal stress bearing elements, while the resin protects fibres to transfer stresses among them. When the properties of the constituent materials (fibres, matrix) and their volume fraction are known, basic mechanical properties of FRP materials may be estimated. This may be achieved by applying the “rule of mixtures” simplification as follows (FIB, 2001)

$$E_{fc} = E_f V_f + E_m V_m \quad (3)$$

$$f_{fc} \approx f_{fr} V_f + f_m V_m \quad (4)$$

where E_{fc} is the modulus of elasticity of the cured FRP in fibre direction, E_f is the modulus of elasticity of fibres, E_m is the modulus of elasticity of the matrix, V_f is the volume fraction of fibres, V_m is the volume fraction of the matrix, f_{fc} is the tensile strength of the cured FRP in fibre direction, f_{fr} is the tensile strength of fibres, and f_m is the tensile strength of the matrix. In the above equations, $V_f + V_m = 1$. Fig. 7 shows the stress-strain curve used in this study for the CFRP composites in the direction of the fibre.

Table 1 contains the mechanical properties of CFRP sheets (MBrace CF 130) based on the fibre properties provided from the supplier. In this table, t_f , ϵ_{fr} , and ν_f are the thickness, ultimate tensile strain, and Poisson’ ratio of fibres respectively. Because the thickness of the fibre ($t_f = 0.165$ mm)

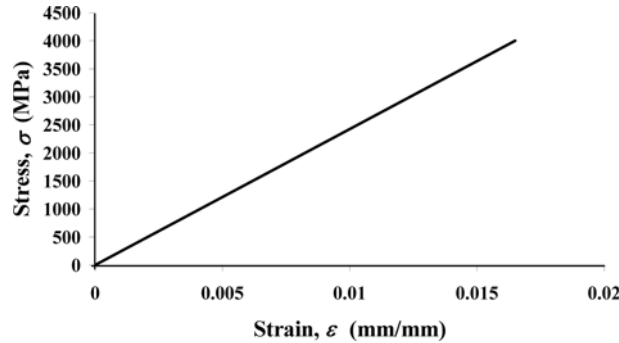


Fig. 7 Representative stress-strain curve from tensile test data, MBrace CF 130 carbon fibre (MBT 2002)

Table 1 Mechanical properties of the CFRP sheet (MBrace CF 130) based on the fibre properties provided from the supplier and the cured sheet

t_f (mm)	f_{fr} (Mpa)	E_f (GPa)	ϵ_{fr} (mm/mm)	ν_f
0.165	3900	240	0.0155	0.2
t_{fc} (mm)	f_{fr} (Mpa)	E_{fc} (GPa)	ϵ_{frc} (mm/mm)	ν_{fc}
1	643.5	39.6	0.0155	0.2

c suffix = Cured sheet

was very small compared to the element dimensions and this causes a low aspect ratio in the FE model, mechanical properties of the cured CFRP sheet were modified based on the cured thickness ($t_{fc} = 1$ mm) using Eqs. (3) and (4). For this, it was considered that $V_f + V_m = 1 \text{ mm}^3$ for a 1 mm^2 FRP cured sheet and $V_f = 0.165 \text{ mm}^3$ for a 1 mm^2 FRP sheet. Moreover, the modulus of elasticity and the tensile strength of the matrix, E_m and f_m , were assumed to be zero because of their small values in comparison to the fibre’s modulus and strength for simplicity. Table 1 also contains the modified mechanical properties of the cured CFRP sheet. In this table, ϵ_{frc} and ν_{fc} are the ultimate tensile strain and the Poisson’s ratio of the cured CFRP sheet respectively.

Two different representations can be used in order to model the FRP that is bonded to RC elements. These are: (1) linear elastic up to failure considering FRPs as an isotropic material; and (2) considering the FRPs as an orthotropic material with anisotropic plasticity. Although the first model is simple, it cannot consider the FRPs’ compressive strength. Since in the web-bonded system, FRPs are subjected to tension and compression simultaneously and because the properties of FRPs are different in tension and in compression, by using this model, ANSYS considers the properties for FRPs in compression similar to those in tension, which is not desirable for analysing the web-bonded FRP structures. To solve this problem, ANSYS offers an anisotropic modelling called ANISO, which allows the introduction of the mechanical properties of FRPs in tension and compression in different directions (x , y , and z). In this model, a modified von Mises yield criterion is used. It is assumed that the principal axes of anisotropy coincide with the material (or element) coordinate system and remains unchanged during the loading. The material behaviour is described by the uniaxial tensile and compressive stress-strain curves and also the shear stress-strain curves in

Table 2 Summary of material properties of the cured CFRP sheet

t_{fc} (mm)	E_x (Mpa)	E_y (GPa)	E_z (GPa)	ν_{xy}	ν_{yz}	ν_{xz}	G_{xy} (GPa)	G_{yz} (GPa)	G_{xz} (GPa)
1	39600	3065.86	3065.86	0.2	0.3	0.2	2075.14	2075.14	1179.20

Table 3 Summary of material properties of the cured CFRP sheet in the anisotropic modelling

Value*	X	Y	Z
Tensile yield stresses (MPa)	643.5	8.86	8.86
Tangent moduli in tension (Mpa)	0	0	0
Compressive yield stresses (MPa)	13.20	13.20	13.20
Tangent moduli in compression (Mpa)	0	0	0
Shear yield stresses (MPa)	6.93	6.93	6.93
Tangent moduli after shear yielding (Mpa)	0	0	0

Note: * All values are based on the thickness of the cured CFRP sheet equal to 1 mm.

three orthogonal directions: x , y , and z . A bilinear material model in each direction is assumed so that the initial slope of the curve is taken as the elastic moduli of the material and then, at the specified yield stress, the curve continues along the second slope defined by the tangent modulus. This value cannot be less than zero or greater than the elastic modulus. Because the stress-strain behaviour of FRPs is linear up to failure, they do not have any specified yield stresses, and hence no tangent modulus can be defined for these materials. Therefore, in the current study, the ultimate strength of FRPs was taken, as their yield stresses in the ANISO modelling and their tangent modulus was taken to zero. The numerical results of all specimens showed that the stress levels in FRPs were less than their ultimate stress and therefore no errors occurred under these assumptions.

Material properties of the cured CFRP sheet for anisotropic modelling are tabulated in Tables 2 and 3. It should be mentioned that the stress values shown in Table 3 satisfy the consistency condition (ANSYS 2003). Because of the unavailability of the compressive strength of the FRP and because the FRP sheet is bonded to the concrete surface by epoxy adhesives, the compressive strength of the cured sheet was assumed to be equal to the compressive strength of the adhesive, which is conservative for design.

Steel plate was added at the support in the finite element models as a linearly elastic material (as in the actual column) to provide a more even stress distribution over the support areas. Steel plate had a thickness of 25 mm; yield strength of 410 MPa, modulus of elasticity about 200 GPa and a Poisson's ratio of 0.3.

In nonlinear analysis, the total load applied to a finite element model is divided into a series of load increments called "load steps". When the solution is completed at each increment, the stiffness matrix of the model is updated to reflect nonlinear changes in structural stiffness before proceeding to the next load increment. The ANSYS program uses Newton-Raphson equilibrium iterations for adjusting the model stiffness. The Newton-Raphson iterative method provides convergence at the end of each load increment within the specified tolerance limits. In the ANSYS program, automatic time stepping predicts and controls the load step sizes. If the convergence behaviour based on the former solution history and the physics of the model is smooth, automatic time stepping will

increase the load increment up to a selected maximum load step size. If the convergence behaviour is not smooth enough, automatic time stepping will reduce the load increment until it is equal to a selected minimum load step size. For the automatic time stepping, the maximum and minimum load step sizes are required. In the current study, the load step sizes were adjusted, depending on the specimen's behaviour. If convergence did not occur, the number of substeps was increased. In case, the force convergence was still unachievable, the convergence tolerance was relaxed. For this, the convergence tolerance limits were increased to a maximum of 5 times the default tolerance limits (0.5% for force checking and 5% for displacement checking). In order to help with the convergence, a strategy was to apply displacements to the system rather than the loads. The forces required to produce these pre-chosen displacements were then considered as the beam-tip loads. The entire load-displacement curves of the specimens were captured at the end of the analysis using this strategy.

4. Comparison between experimental and numerical results

In this section, the numerical results for all specimens are presented and compared with experimental values.

The stress distribution obtained from finite element analysis of the steel plate is shown in Fig. 8. As is seen, the maximum normal stress is about 305 MPa, which is 25% less than the plate yield strength, and hence the assumed linear behaviour is justified.

In the following, strain contours in plain and retrofitted specimens RSM1 and RSM2, and the stress contours in the CFRP sheet in these specimens are presented, followed by a comparison between the failure mechanisms of the plain specimen, CSM0, repaired specimens, RPSM1 and RPSM2, and retrofitted specimen, RSM2, obtained numerically and the failure mechanisms observed experimentally. Subsequently, comparisons between load-displacement curves obtained from ANSYS and the experimental data are presented.

The strain contours in the body of the specimens CSM0, RSM1, and RSM2 are shown in Figs. 9-11 respectively, indicating their failure mechanisms. As is seen, the plain control specimen, CSM0, and the retrofitted specimen, RSM1, have developed very high stresses at the column face. This

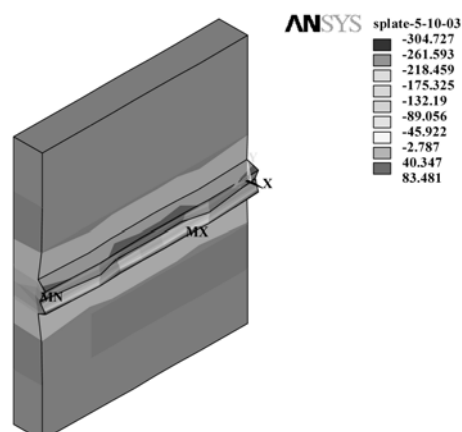


Fig. 8 Stress distribution in the steel plate at ultimate

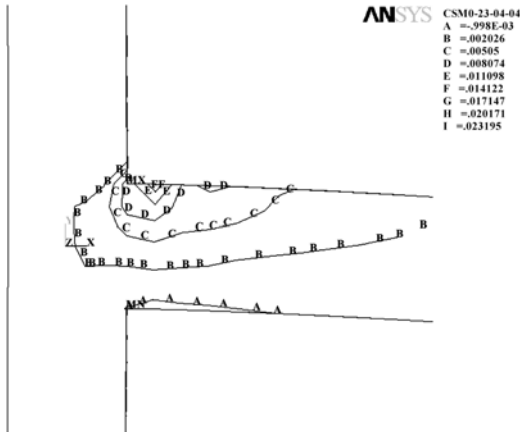


Fig. 9 Strain contour in concrete (CSM0)

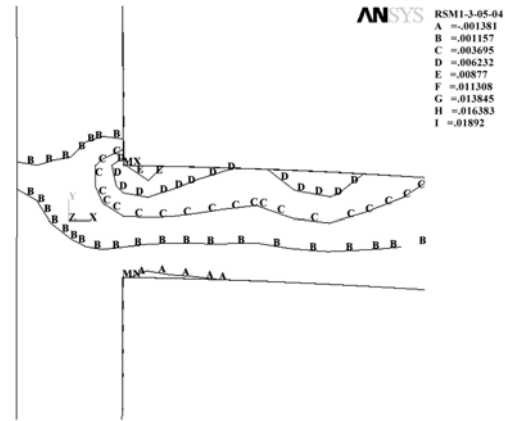


Fig. 10 Strain contour in concrete (RSM1)

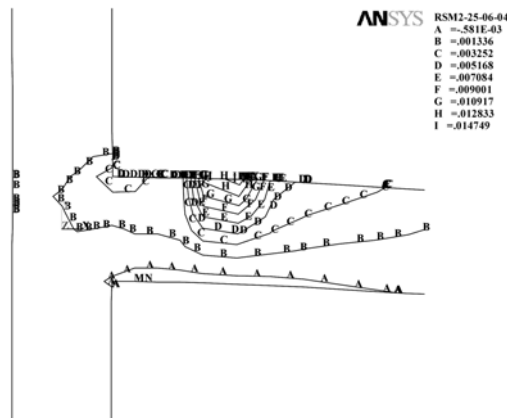


Fig. 11 Strain contour in concrete (RSM2)

reassures the validity of the numerical solution as all these specimens failed experimentally at the column face as well. Fig. 11 illustrates the strain distribution along the beam in the retrofitted specimen, RSM2. As is seen, large strains were concentrated at the cut-off point of CFRP, which shows that the failure occurred at this point without any considerable deformation at the column face. The plain specimen CSM0 has a maximum compressive strain of 0.0023 mm/mm, which is very close to the ultimate strain of 0.003 mm/mm. It shows that the failure occurred due to steel yielding in tension followed by development of large strains in concrete and concrete crushing in the compression zone. A similar behaviour is observed for specimen RSM1, which failed at the same locations. Specimen RSM2 exhibits a maximum strain of 0.0016 mm/mm, which is about 50% of the ultimate strain, and the large deformation is localised at the cut-off point of CFRP with a maximum strain of 0.015 mm/mm.

Stress distributions in the CFRP sheets are illustrated in Figs. 12 and 13 for specimens, RSM1, and RSM2 respectively. As is seen, in specimen RSM1, which was wrapped with only one ply CFRP, the maximum tensile stress was 409 MPa, which is about 60% of the ultimate tensile strength of CFRP. It indicates that CFRPs were intact up to the ultimate load and the failure was

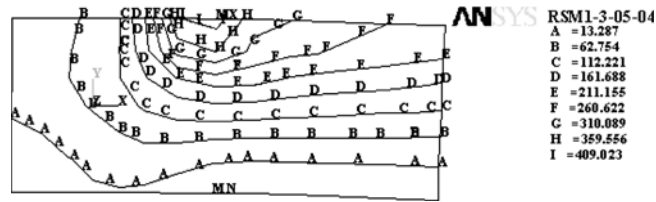


Fig. 12 Stress contour in CFRP (RSM1)

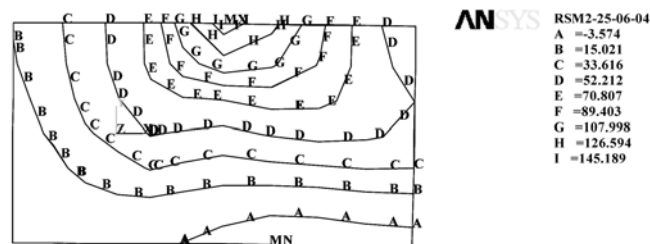


Fig. 13 Strain contour in CFRP (RSM2)

caused by concrete crushing at the column face followed by the beam rotation about the fulcrum and the rupture of CFRP on the tension side, as discussed in Mahini *et al.* (2004) and Ronagh and Mahini (2005). On the other hand, the maximum compressive stress in CFRP is about 13.28 MPa, which is close to the maximum compressive strength of 13.20 MPa. It shows that the proposed anisotropic model has been able to simulate the actual performance of CFRP wrap. Similar trends are observed in the compression zones of CFRPs in specimen RSM2 with the maximum tensile stress being 145 MPa. This trend was expected because of the use of three CFRP plies in this specimen.

Comparisons between the numerical predictions for the failure mechanisms of specimens CSM0, RPSM2, and RSM2 and their experimental counterpart are shown in Figs. 14-17 respectively. Good agreements between the results are observed, which indicates that the numerical analysis could be used as a practical tool for the analysis of repaired/retrofitted beam-column joints that encompass a web-bonded FRP system.

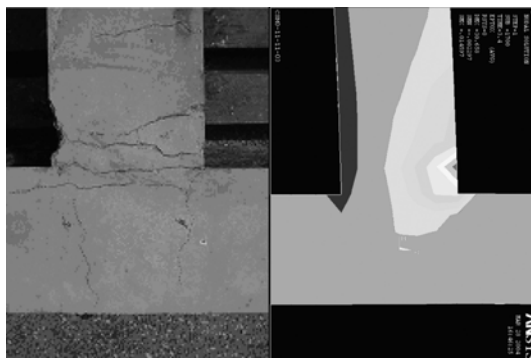


Fig. 14 Experimental versus numerical failure mechanism (CSM0)

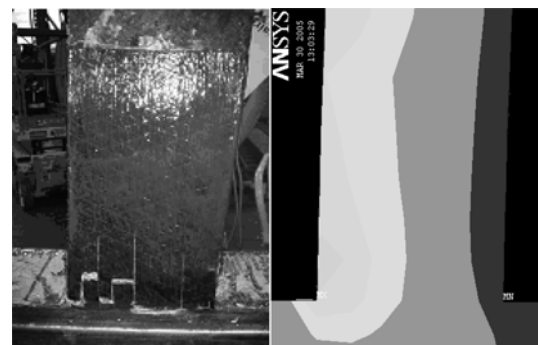


Fig. 15 Experimental versus numerical failure mechanism (RPSM1)

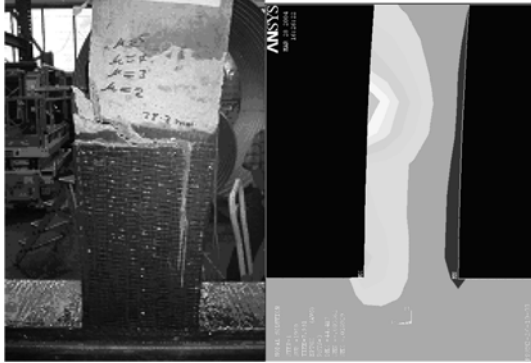


Fig. 16 Experimental versus numerical failure mechanism (RPSM2)



Fig. 17 Experimental versus numerical failure mechanism (RSM2)

Figs. 18-22 contain a comparison between the load-displacement curves predicted by ANSYS and the test results for all specimens. As is seen, the agreement is reasonable. The results of ANSYS match the plain specimen better than the repaired/retrofitted specimens. This may be a result of bond slip between FRP, steel reinforcements and concrete that is ignored in the current analysis. Also, as Figs. 19 and 20 show, the initial slope of the numerical load-displacement curves for specimens RPSM1 and RPSM2 are more than those obtained from the experiments, because these specimens were already cracked but were assumed to be uncracked in FE modelling.

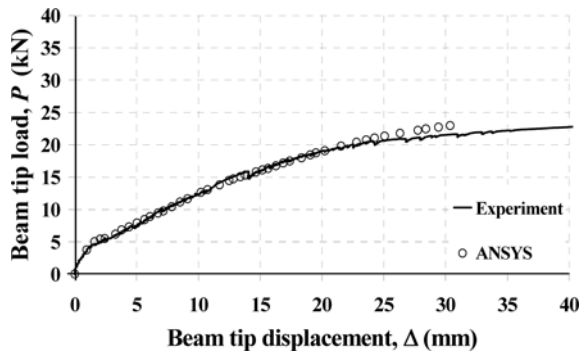


Fig. 18 Load-displacement curves (CSM0)

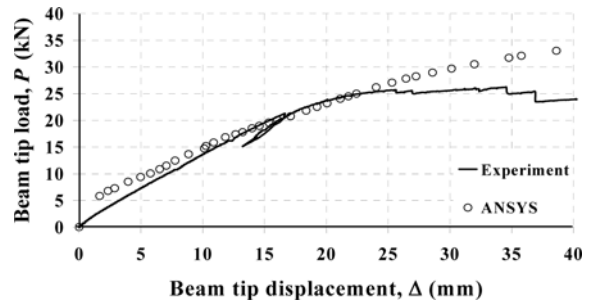


Fig. 19 Load-displacement curves (RPSM1)

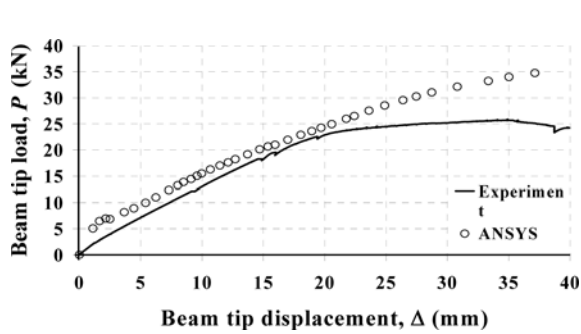


Fig. 20 Load-displacement curves (RPSM2)

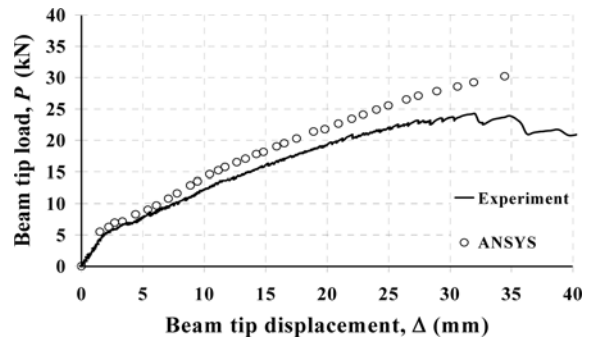


Fig. 21 Load-displacement curves (RSM1)

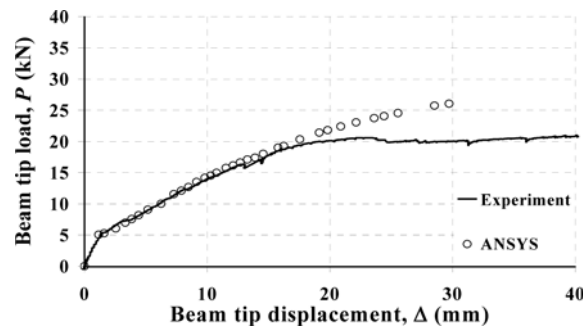


Fig. 22 Load-displacement curves (RSM2)

5. Conclusions

Comparison between numerical predictions and experimental results demonstrated a good agreement. This shows that ANSYS can be used as a tool in order to understand the behaviour and to design appropriate amount of CFRP in order to relocate the plastic hinge while maintaining a ductile failure mode.

Numerical predictions as well as the tests showed three types of failures: 1) flexural failure at the beam-end facing to the column and penetration of the yield into the joint core (specimens CSM0, RPSM1, and RSM1); 2) localised beam hinging zone, where a flexural plastic hinge formed at a certain distance from the column face, but spread over a short segment of the beam (specimen RSM2); and 3) distributed beam hinging, where a localised beam hinging zone started at a distance from the face of the column and then distributed over a considerable length of the beam (specimen RPSM2). The results demonstrate that the web-bonded CFRP system can be effectively used to control the location of the plastic hinge in RC moment resisting frames.

Acknowledgements

The first author was supported by a combined IPRS-UQIPRS scholarship from the Australian Federal government and the University of Queensland for the duration of his PhD. The support that enabled him to perform the current research is gratefully acknowledged.

References

- ACI318 (2002), *Building Code Requirements for Structural Concrete*, American Concrete Institute.
- ANSYS, I. (2003), "ANSYS Manual Set", ANSYS Inc., Canonsburg, PA 15317, USA.
- AS3600 (2001), *Concrete Structures*, Standards Australia.
- Baglin, P.S. and Scott, R.H. (2000), "Finite element modelling of reinforced concrete beam-column connections", *ACI Struct. J.*, **97**(6), 886-894.
- FIB (2001), "Externally bonded FRP reinforcement for RC structures", *Bulletin 14*, Federal Institute of Technology Lausanne, Patras.
- Kachlakev, D., Miller, T., Chansawat, K. and Potisuk, T. (2001), "Finite element modeling of reinforced concrete structures strengthened with FRP laminates", *SPR 316*, Oregon Department of Transportation Research Group

- 200 Hawthorne SE, Suite B-240 Salem, and Federal Highway Administration 400 Seventh Street SW Washington, DC 20590.
- Kwak, H.G. and Fillippou, F. (1990), "Finite element analysis of reinforced concrete structures under monotonic loads", Tech. Report No.UCB/SEMM-90/14, Dept. of Civil Engineering, University of California, Berkeley, California.
- Mahini, S.S. and Ronagh, H.R. (2006), "Ductility of FRP-repaired RC beam-column joints", *Proc. of the Second International Conference on Concrete Repair*, Concrete Solutions, June 27-29, St-Malo, France, 123-130.
- Mahini, S.S., Ronagh, H.R. and Dux, P.F. (2004), "Flexural repair of RC exterior beam-column joints using CFRP sheet", *Proceeding of the Second International Conference on FRP Composites in Civil Engineering*, Adelaide, Australia, 8-10 December, 653-658.
- MBT (2002), "MBrace, composite strengthening system", Master Builders Technologies, MBT (Australia) Pty Ltd.
- Noor, F.A. and Boswell, L.F. (1992), *Small Scale Modelling of Concrete Structures*. Elsevier Applied Science.
- Park, R. and Paulay, T. (1975), *Reinforced Concrete Structures*, John Wiley and Sons, Christchurch.
- Parvin, A. and Granata, P. (2000), "Investigation on the effects of fibre composites at concrete joints", *Compos. Part B-Eng.*, **31**(6-7), 499-509.
- Paulay, T. and Priestley, M.J.N. (1992), *Seismic Design of Reinforced Concrete and Masonry Buildings*, John Wiley and Sons, Inc.
- Ronagh, H.R. and Mahini, S.S. (2005), "Upgrading of reinforced concrete joints with carbon fibre sheets", *Proceeding of the Second International Conference on Concrete and Development*, Tehran, April 30-May 2, 2005, CD2-037.
- Vollum, R.L. (1998), "Design and analysis of reinforced concrete beam-column joints", Ph.D., Imperial College, London.
- William, K.J. and Warnke, E.D. (1975), "Constitutive model for the triaxial behaviour of concrete", *International Association for Bridge and Structural Engineering, ISMES*, Bergamo, Italy, 174.

Notation

The following symbols are used in this paper:

E_c/E	: modulus of elasticity of concrete
E_m	: modulus of elasticity of matrix
E_f	: modulus of elasticity of fibre of FRP sheet
E_{fc}	: modulus of elasticity of cured FRP sheet
E_s	: modulus of elasticity of steel bar/steel plate
E_x	: modulus of elasticity of orthotropic material in x direction
E_y	: modulus of elasticity of orthotropic material in y direction
E_z	: modulus of elasticity of orthotropic material in z direction
f_c'	: cylinder compressive strength of concrete
f_{fr}	: tensile strength of fibre of FRP sheet
f_{frc}	: tensile strength of the cured FRP sheet in fibre direction
f_r	: modulus of rupture of concrete (ultimate uniaxial tensile strength of concrete)
f_m	: tensile strength of matrix
f_t	: uniaxial tensile cracking stress in concrete
G_{xy}	: shear modulus of orthotropic material in x-y plane
G_{xz}	: shear modulus of orthotropic material in x-z plane
G_{yz}	: shear modulus of orthotropic material in y-z plane
R^t	: secant modulus
t_f	: thickness of fibre sheet/thickness of FRP wrap based on fibre thickness
t_{fc}	: thickness of cured FRP sheet/thickness of FRP wrap based on the thickness of cured FRP
T_c	: multiplier for the amount of tensile stress relaxation
V_f	: volume fraction of fibres

V_m	: volume fraction of matrix
β_t	: shear transfer coefficient for opened cracks
β_c	: shear transfer coefficient for closed cracks
ε_c'	: strain corresponding to the in the concrete compressive strength f_c'
ε_c	: compressive strain in the extreme fibre of concrete
ε_{cu}	: ultimate compressive strain of concrete
ε_{fr}	: strain of fibre of FRP sheet at ultimate
ε_{frc}	: strain of cured FRP sheet at ultimate
ε^{ck}	: crack strain
ν_f	: Poisson's ratio of fibre of FRP sheet
ν_{fc}	: Poisson's ratio of cured FRP sheet
ν_c	: Poisson's ratio of concrete
ν_s	: Poisson's ratio of steel reinforcement/steel plate
ν_{xy}	: major Poisson's ratio of orthotropic materials in x - y plane
ν_{xz}	: Poisson's ratio of orthotropic material in x - z plane
ν_{yz}	: Poisson's ratio of orthotropic material in y - z plane
ρ	: mass density of concrete